electronics

MDPI

Article

Acoustic-Based Fault Diagnosis of Commutator Motor

Adam Glowacz

Department of Automatic Control and Robotics, Faculty of Electrical Engineering, Automatics, Computer Science and Biomedical Engineering, AGH University of Science and Technology, al. A. Mickiewicza 30, 30-059 Kraków, Poland; adglow@agh.edu.pl

Received: 4 October 2018; Accepted: 2 November 2018; Published: 5 November 2018

Abstract: In the paper, the author presents acoustic-based fault diagnosis of a commutator motor (CM). Five states of the commutator motor were considered: healthy commutator motor, commutator motor with broken rotor coil, commutator motor with shorted stator coils, commutator motor with broken tooth on sprocket, commutator motor with damaged gear train. A method of feature extraction MSAF-15-MULTIEXPANDED-8-GROUPS (Method of Selection of Amplitudes of Frequency Multiexpanded 8 Groups) was described and implemented. Classification methods, such as nearest neighbour (NN), nearest mean (NM), self-organizing map (SOM), backpropagation neural network (BNN) were used for acoustic analysis of the commutator motor. The paper provides results of acoustic analysis of the commutator motor. The results had a good recognition rate. The results of acoustic analysis were in the range of 88.4–94.6%. The NM classifier and the MSAF-15-MULTIEXPANDED-8-GROUPS provided TE_{RCM} = 94.6%.

Keywords: commutator motor; fault diagnosis; method; technique; signal processing; acoustic

1. Introduction

Fault diagnosis of electrical rotating motors has been extensively investigated since the 20th century, and can increase the reliability and safety of electrical rotating motors. Condition monitoring of electrical motors are very important for industry, reducing loss due to unforeseen faults and damage. Unforeseen faults and damage of electrical rotating motors lead to the loss of production and income. Unfortunately, stator and rotor are the most important components in electrical rotating motors. Stator and rotor faults appear very often. Stators and rotors of electrical rotating motors must be monitored. Condition monitoring guarantees safe operation of machines and prevents unforeseen breakdowns. Acoustic signals contain a lot of diagnostic information, and can be used for detection of faults. Therefore, acoustic signals and signal processing methods should be deeply studied for proper recognition. Scientists developed many diagnostic methods of fault diagnosis. They are used for various types of machines and faults. Faults of electrical rotating motors (stator faults, rotor faults, broken rotor bar, ring cracking, bearing failures, rotor shaft failure, air-gap irregularities, broken teeth on sprocket) can be diagnosed by vibration [1–12] and acoustic signals [13–22]. Electric current analysis [23–31] and thermal analysis [32–34] are mostly used for limited faults, such as stator faults, rotor faults, and bearing failures. Acoustic signals are difficult to process, because they are very noisy (for example, several operating motors generate many acoustic signals). The advantage of acoustic-based fault diagnosis is non-invasive measurement (for example, we can measure an acoustic signal two meters from the machine). Vibration-based fault diagnosis is similar, but we have to put our measuring device close to the machine. Vibration signals are less noisy than acoustic signals.

The paper presents acoustic-based fault diagnosis of the commutator motor (CM). Five states of the commutator motor (CM) were considered: CM with shorted stator coils (Figures 1a and 2a), CM with broken rotor coil (Figures 1b and 2b), healthy CM (Figure 1c), CM with broken tooth on sprocket (Figure 3), CM with damaged gear train (Figure 4).

Figure 1. (**a**) Commutator motor (CM) with shorted stator coils; (**b**) CM with broken rotor coil; (**c**) healthy CM.

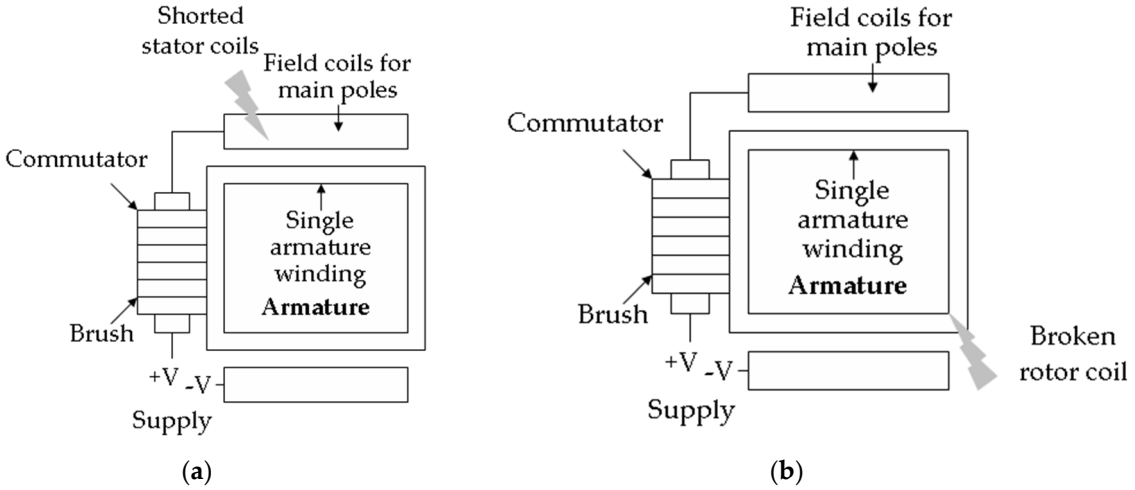

Figure 2. (**a**) CM with shorted stator coils; (**b**) CM with broken rotor coil.

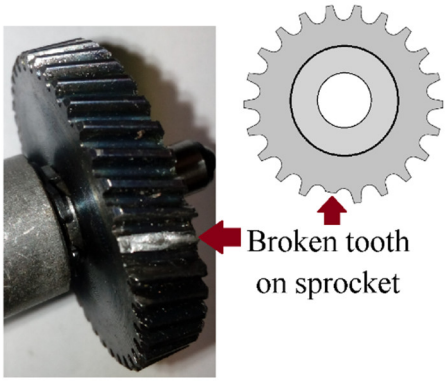

Figure 3. Broken tooth on sprocket of the electric impact drill.

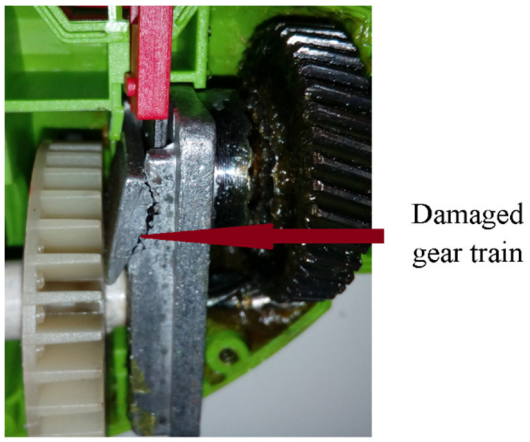

Figure 4. Damaged gear train of the electric impact drill.

The described approach consists of methods of signal processing, such as amplitude normalization, FFT, the MSAF-15-MULTIEXPANDED-8-GROUPS, nearest neighbour (NN), or nearest mean (NM) or SOM (self-organizing map) or BNN (backpropagation neural network). The paper provided the results of acoustic analysis of the CM.

2. Acoustic-Based Fault Diagnosis Technique of the Commutator Motor

Acoustic-based fault diagnosis technique was based on pattern recognition. It used a pre-processing step, feature extraction step, and classification step. A block diagram of acoustic-based fault diagnosis technique was shown in Figure 5.

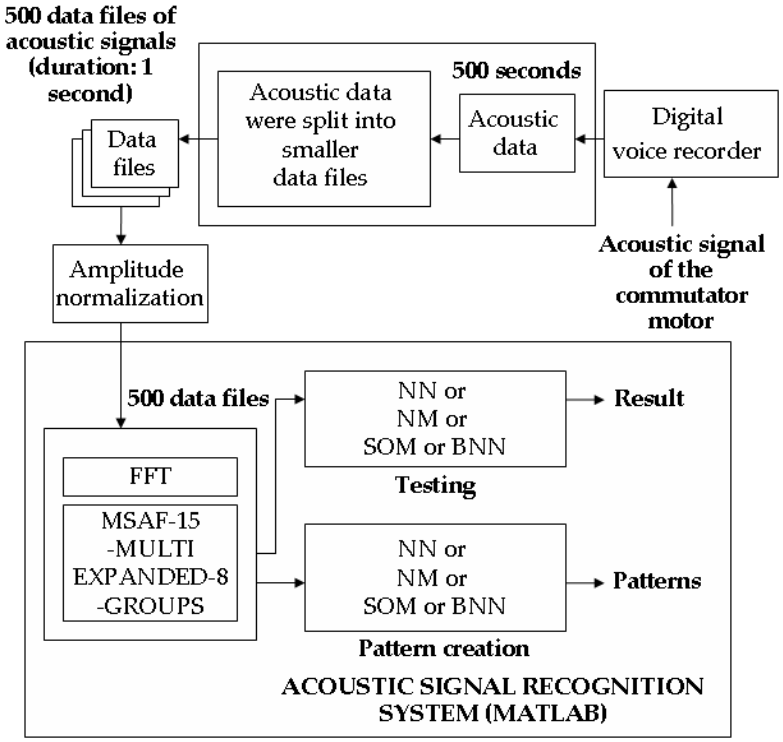

Figure 5. Flowchart of acoustic-based fault diagnosis techniques of the CM using the MSAF-15-MULTIEXPANDED-8-GROUPS.

Acoustic signals were measured using ZALMAN ZM-MIC1 microphone. The following steps of signal processing were used: recording of acoustic signal of the CM, split of soundtrack into

smaller data files, amplitude normalization, FFT, the MSAF-15-MULTIEXPANDED-8-GROUPS, NN classifier or NM classifier or SOM or BNN. Recording of the acoustic signal of the CM was carried out using digital voice recorder (format: WAVE, number of channel-1, sampling frequency-44,100 Hz). There was also possibility to record acoustic signals using a capacity microphone with a computer (Figures 6 and 7). Next, splitting the soundtrack into smaller data files was carried out. The obtained data files (1 second samples) were processed by amplitude normalization, windowing (window size of 32,768), FFT, and the MSAF-15-MULTIEXPANDED-8-GROUPS. The MSAF-15-MULTIEXPANDED-8-GROUPS selected 1–15 frequency components, forming feature vectors consisting of 1–15 frequency components. Computed feature vectors were used for pattern creation and testing. Methods such as NN, NM, SOM, and BNN were used for data classification.

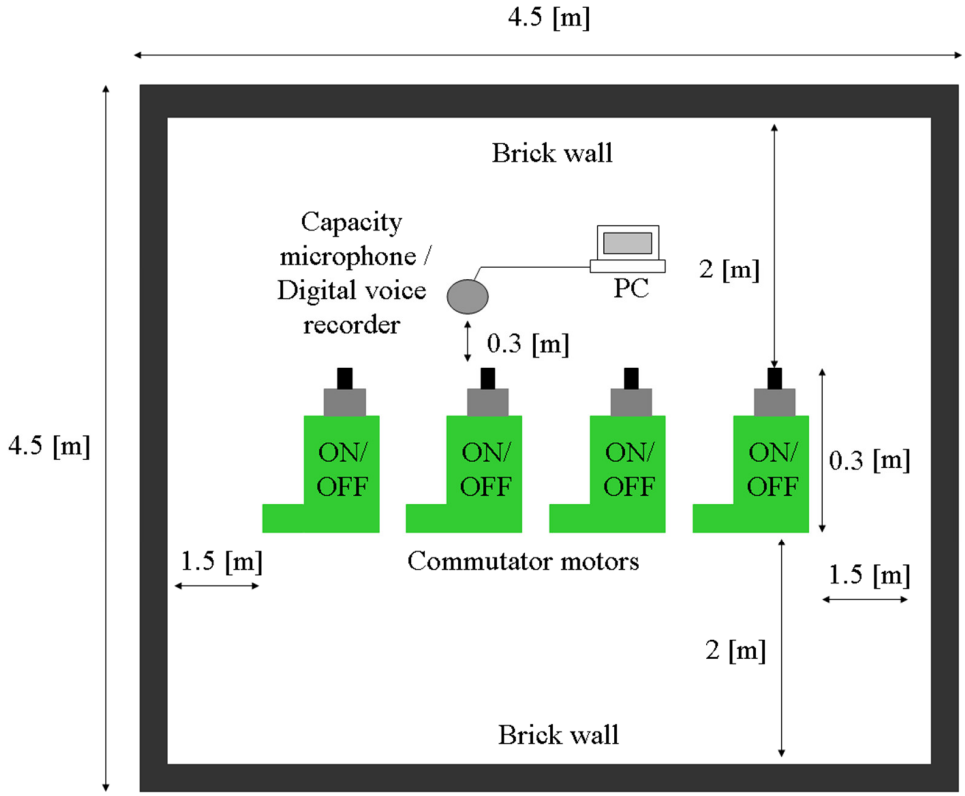

Figure 6. Experimental setup of analysis of acoustic signals of commutator motors.

Figure 7. Capacity microphone (ZALMAN ZM-MIC1 microphone) and the commutator motor (electric impact drill).

2.1. Method of Selection of Amplitudes of Frequency Multiexpanded 8 Groups

The Method of Selection of Amplitudes of Frequency Multiexpanded 8 Groups (MSAF-15-MULTIEXPANDED-8-GROUPS) depended on differences of spectra of acoustic signals. Differences of spectra of acoustic signals depended on generated acoustic signals of the CM. Generated acoustic signals depended on type of the motor, motor size, rotor speed, and analysed faults of the motor. The author analysed 5 states of the CM (healthy CM, CM with broken rotor coil, CM with shorted stator coils, CM with broken tooth on sprocket, and CM with damaged gear train). Steps of the MSAF-15-MULTIEXPANDED-8-GROUPS were listed below:

1. Compute frequency spectra of acoustic signals of commutator motors (the author used 6 one-second samples for state A, 6 one-second samples for state B, 6 one-second samples for state C, 6 one-second samples for state D). Computed frequency spectrum of state A (healthy CM) was described as vector of 16,384 elements **hcm** = [hcm_1, hcm_2, ..., hcm_{16384}]. Computed frequency spectrum of state B (CM with broken rotor coil) was denoted as vector of 16,384 elements **cmbrc** = [$cmbrc_1$, $cmbrc_2$, ..., $cmbrc_{16384}$]. Computed frequency spectrum of state C (CM with shorted stator coils) was expressed as vector of 16,384 elements **cmssc** = [$cmssc_1$, $cmssc_2$, ..., $cmssc_{16384}$]. Computed frequency spectrum of state D (CM with broken tooth on sprocket) was expressed as vector of 16384 elements **cmbts** = [$cmbts_1$, $cmbts_2$, ..., $cmbts_{16384}$]. Computed frequency spectrum of state E (CM with damaged gear train) was expressed as vector of 16,384 elements **cmdgt** = [$cmdgt_1$, $cmdgt_2$, ..., $cmdgt_{16384}$].
2. Compute differences of computed frequency spectra of states A, B, C, D, E: **hcm** − **cmbrc**, **hcm** − **cmssc**, **cmbrc** − **cmssc**, **cmbts** − **hcm**, **cmbts** − **cmbrc**, **cmbts** − **cmssc**, **cmdgt** − **hcm**, **cmdgt** − **cmbrc**, **cmdgt** − **cmssc**, **cmdgt** − **cmbts**.
3. Compute absolute values: |**hcm** − **cmbrc**|, |**hcm** − **cmssc**|, |**cmbrc** − **cmssc**|, |**cmbts** − **hcm**|, |**cmbts** − **cmbrc**|, |**cmbts** − **cmssc**|, |**cmdgt** − **hcm**|, |**cmdgt** − **cmbrc**|, |**cmdgt** − **cmssc**|, |**cmdgt** − **cmbts**|.
4. Select 15 maximum differences of computed frequency spectra of states A, B, C, D, E: $\max_1$(|**hcm** − **cmbrc**|), $\max_2$(|**hcm** − **cmbrc**|), ..., $\max_{15}$(|**hcm** − **cmbrc**|), $\max_1$(|**hcm** − **cmssc**|), $\max_2$(|**hcm** − **cmssc**|), ..., $\max_{15}$(|**hcm** − **cmssc**|), $\max_1$(|**cmbrc** − **cmssc**|), $\max_2$(|**cmbrc** − **cmssc**|), ..., $\max_{15}$(|**cmbrc** − **cmssc**|), $\max_1$(|**cmbts** − **hcm**|), $\max_2$(|**cmbts** − **hcm**|), ..., $\max_{15}$(|**cmbts** − **hcm**|), $\max_1$(|**cmbts** − **cmbrc**|), $\max_2$(|**cmbts** − **cmbrc**|), ..., $\max_{15}$(|**cmbts** − **cmbrc**|), $\max_1$(|**cmbts** − **cmssc**|), $\max_2$(|**cmbts** − **cmssc**|), ..., $\max_{15}$(|**cmbts** − **cmssc**|), $\max_1$(|**cmdgt** − **hcm**|), $\max_2$(|**cmdgt** − **hcm**|), ..., $\max_{15}$(|**cmdgt** − **hcm**|), $\max_1$(|**cmdgt** − **cmbrc**|), $\max_2$(|**cmdgt** − **cmbrc**|), ..., $\max_{15}$(|**cmdgt** − **cmbrc**|), $\max_1$(|**cmdgt** − **cmssc**|), $\max_2$(|**cmdgt** − **cmssc**|), ..., $\max_{15}$(|**cmdgt** − **cmssc**|), $\max_1$(|**cmdgt** − **cmbts**|), $\max_2$(|**cmdgt** − **cmbts**|), ..., $\max_{15}$(|**cmdgt** − **cmbts**|). The result of feature extraction method MSAF-15 is the vector consisted of 1–15 frequency components. Let us see following example using the MSAF-15. There are 5 states of the CM: A, B, C, D, E. Five frequency spectra of acoustic signals of the CM ((FS-A), (FS-B), (FS-C), (FS-D), (FS-E)-frequency spectra of states A, B, C, D, E) were computed. The MSAF-15 computed frequency components 100, 160, 200, 260, 300 Hz for difference |(FS-A) − (FS-B)|. The MSAF-15 computed frequency components 120, 160, 210, 260, 310 Hz for difference |(FS-A) − (FS-C)|. The MSAF-15 computed frequency components 120, 170, 220, 230, 310 Hz for difference |(FS-B) − (FS-C)|. The MSAF-15 computed frequency components 400, 410, 420, 430, 440 Hz for difference |(FS-D) − (FS-A)|. The MSAF-15 computed frequency components 405, 415, 425, 435, 445 Hz for difference |(FS-D) − (FS-B)|. The MSAF-15 computed frequency components 410, 415, 420, 425, 430 Hz for difference |(FS-D) − (FS-C)|. The MSAF-15 computed frequency components 500, 505, 510 Hz for difference |(FS-E) − (FS-A)|. The MSAF-15 computed frequency components 515, 520, 525 Hz for difference |(FS-E) − (FS-B)|. The MSAF-15 computed frequency components 530, 540, 550 Hz for difference |(FS-E) − (FS-C)|. The MSAF-15 computed frequency components 560, 570, 580 Hz for difference |(FS-E)

− (FS-D)|. None of common frequency components were selected for the presented example. The MSAF-15-MULTIEXPANDED-GROUPS extends the MSAF-15 method. A parameter called *TCoF-TS* (Threshold of common frequency components-training sets) was used. This parameter was defined as: *TCoF-TS* = (number of required common frequency components of analysed training sets)/(number of analysed differences).

5. Set the parameter *TCoF-TS*. This parameter affects the number of common frequency components. Let us consider following example using the MSAF-15-MULTIEXPANDED. Four training sets of acoustic training samples are given: (A1, B1, C1, D1, E1), (A2, B2, C2, D2, E2), (A3, B3, C3, D3, E3), (A4, B4, C4, D4, E4), where A1, A2, A3, A4—denoted 4 acoustic training samples of state A; B1, B2, B3, B4—denoted 4 acoustic training samples of state B; C1, C2, C3, C4—denoted 4 acoustic training samples of state C; D1, D2, D3, D4—denoted 4 acoustic training samples of state D; E1, E2, E3, E4—denoted 4 acoustic training samples of state E. The MSAF-15-MULTIEXPANDED computed frequency components (FS-A1, FS-B1, FS-C1, FS-D1, FS-E1), (FS-A2, FS-B2, FS-C2, FS-D2, FS-E2), (FS-A3, FS-B3, FS-C3, FS-D3, FS-E3), (FS-A4, FS-B4, FS-C4, FS-D4, FS-E4), where FS-A1, FS-A2, FS-A3, FS-A4—denoted 4 frequency spectra of state A, FS-B1, FS-B2, FS-B3, FS-B4—denoted 4 frequency spectra of state B, FS-C1, FS-C2, FS-C3, FS-C4—denoted 4 frequency spectra of state C, FS-D1, FS-D2, FS-D3, FS-D4—denoted 4 frequency spectra of state D, FS-E1, FS-E2, FS-E3, FS-E4—denoted 4 frequency spectra of state E. Next, 40 differences between frequency spectra are computed: |(FS-A1) − (FS-B1)|, |(FS-A1) − (FS-C1)|, |(FS-B1) − (FS-C1)|, |(FS-D1) − (FS-A1)|, |(FS-D1) − (FS-B1)|, |(FS-D1) − (FS-C1)|, |(FS-E1) − (FS-A1)|, |(FS-E1) − (FS-B1)|, |(FS-E1) − (FS-C1)|, |(FS-E1) − (FS-D1)|, ... , |(FS-A4) − (FS-B4)|, |(FS-A4) − (FS-C4)|, |(FS-B4) − (FS-C4)|, |(FS-D4) − (FS-A4)|, |(FS-D4) − (FS-B4)|, |(FS-D4) − (FS-C4)|, |(FS-E4) − (FS-A4)|, |(FS-E4) − (FS-B4)|, |(FS-E4) − (FS-C4)|, |(FS-E4) − (FS-D4)|. Let us consider following example. If we set *TCoF-TS* = 4/40 = 0.1, then the MSAF-15-MULTIEXPANDED selects frequency components found 4 times for 40 differences. If we set *TCoF-TS* = 6/40 = 0.15, then the MSAF-15-MULTIEXPANDED selects frequency components found 6 times for 40 differences. The MSAF-15-MULTIEXPANDED found frequency component 160 Hz-6 times, frequency component 210 Hz-4 times. The MSAF-15-MULTIEXPANDED selects 160, 210 Hz (if *TCoF-TS* = 4/40 = 0.1). The MSAF-15-MULTIEXPANDED selects 160 Hz (if *TCoF-TS* = 6/40 = 0.15). The MSAF-15-MULTIEXPANDED selects none of frequency components (if *TCoF-TS* = 8/40 = 0.2). The parameter *TCoF-TS* depends on analysed signal.
6. Select groups of common frequency components. The MSAF-15-MULTIEXPANDED-8-GROUPS used 8 groups. Each group of common frequency components consists of the best frequency components for recognition. Let us analyse following example. There are 4 states of the CM: A, B, C, D (for 5 states it will be similarly). The MSAF-15-MULTIEXPANDED-8-GROUPS found: frequency component 210 Hz (4 times), frequency component 160 Hz (6 times), frequency component 400 Hz (7 times). The frequency component 210 Hz is good for recognition of |(FS-A) − (FS-B)|, |(FS-A) − (FS-C)|, |(FS-B) − (FS-C)|. The frequency component 160 Hz is good for recognition of |(FS-D) − (FS-A)|, |(FS-D) − (FS-B)|, |(FS-D) − (FS-C)|. The frequency component 400 Hz is good for recognition of |(FS-A) − (FS-B)|. Essential frequency components are 210 Hz and 160 Hz. The frequency component 400 Hz is not good for analysis. The essential frequency components 160 Hz and 210 Hz form 1 group of essential frequency components.
7. Use 1–8 computed groups.
8. Form a feature vector.

The author presented the MSAF-15-MULTIEXPANDED-8-GROUPS in Figure 8.

The author used 30 one-second training samples for proper pattern creation process. The author used 6 training sets (30 one-second samples). Computed absolute values of differences: |**hcm** − **cmbrc**|, |**hcm** − **cmssc**|, |**cmbrc** − **cmssc**|, |**cmbts** − **hcm**|, |**cmbts** − **cmbrc**|, |**cmbts** − **cmssc**|, |**cmdgt** − **hcm**|, |**cmdgt** − **cmbrc**|, |**cmdgt** − **cmssc**|, |**cmdgt** − **cmbts**| were depicted in Figures 9–18 (rotor speed-3000 rpm, training set 6).

The MSAF-15-MULTIEXPANDED-8-GROUPS found 28 essential frequency components: 48, 50, 79, 81, 97, 101, 128, 157, 159, 1469, 1471, 1672, 1926, 1927, 1934, 1935, 1939, 1942, 1953, 1957, 1958, 1961, 1978, 2038, 2039, 2042, 2059, 2547 Hz for *TCoF-TS* = 0.125 (3/18 = 0.125). Computed essential frequency components were presented in Tables 1–5 (Figures 19–23).

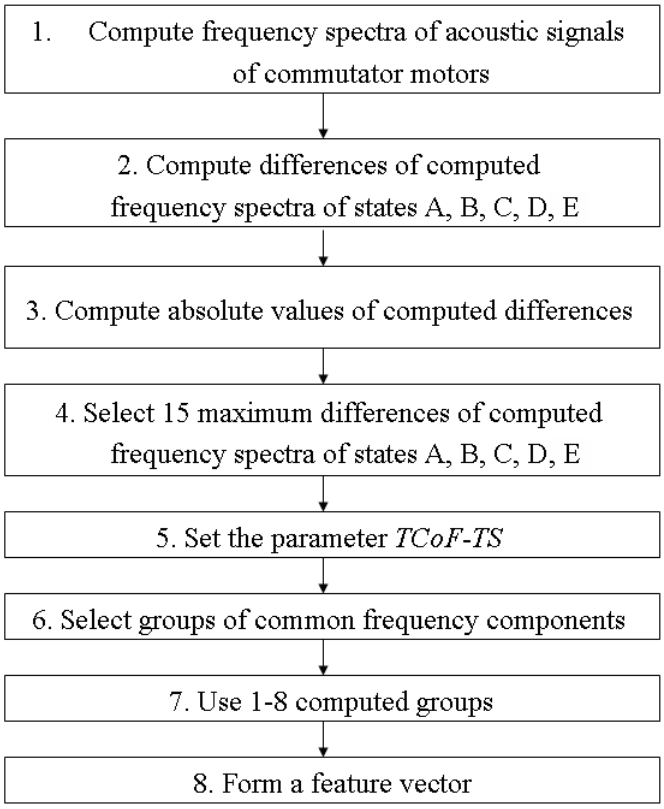

Figure 8. Flowchart of the MSAF-15-MULTIEXPANDED-8-GROUPS.

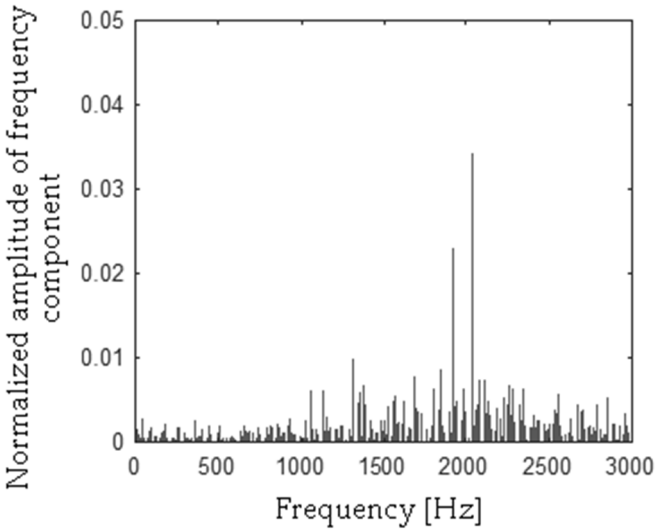

Figure 9. Absolute values of difference of frequency spectra (|**hcm** − **cmbrc**|) using the MSAF-15-MULTIEXPANDED-8-GROUPS.

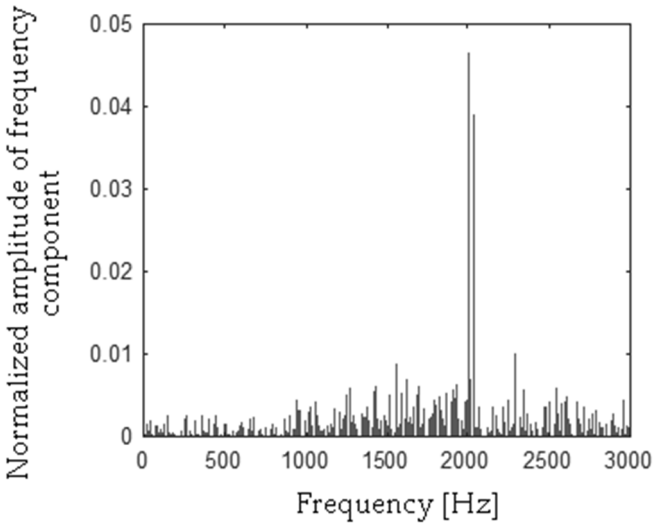

Figure 10. Absolute values of difference of frequency spectra (|**hcm** − **cmssc**|) using the MSAF-15-MULTIEXPANDED-8-GROUPS.

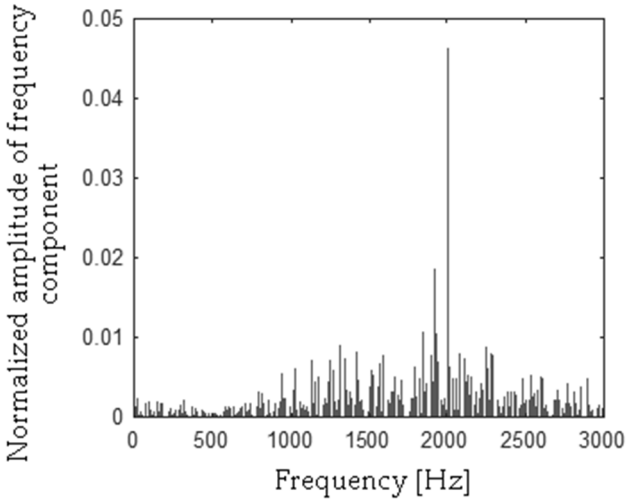

Figure 11. Absolute values of difference of frequency spectra (|**cmbrc** − **cmssc**|) using the MSAF-15-MULTIEXPANDED-8-GROUPS.

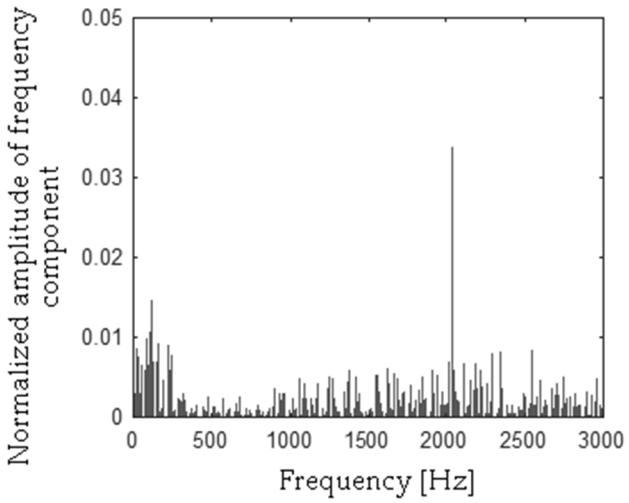

Figure 12. Absolute values of difference of frequency spectra (|**cmbts** − **hcm**|) using the MSAF-15-MULTIEXPANDED-8-GROUPS.

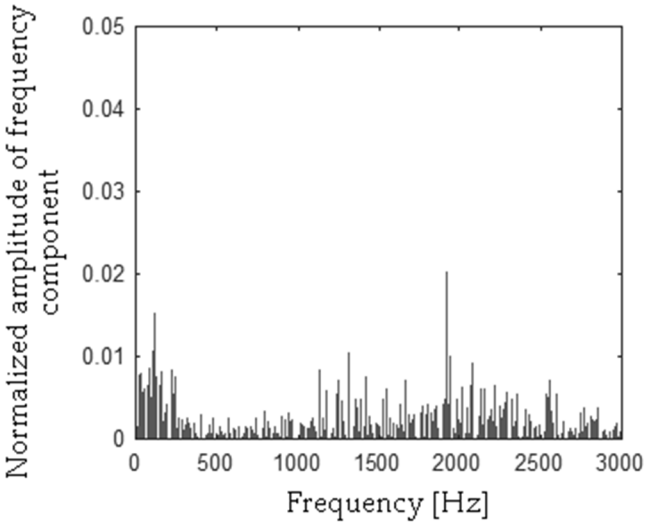

Figure 13. Absolute values of difference of frequency spectra (|**cmbts** − **cmbrc**|) using the MSAF-15-MULTIEXPANDED-8-GROUPS.

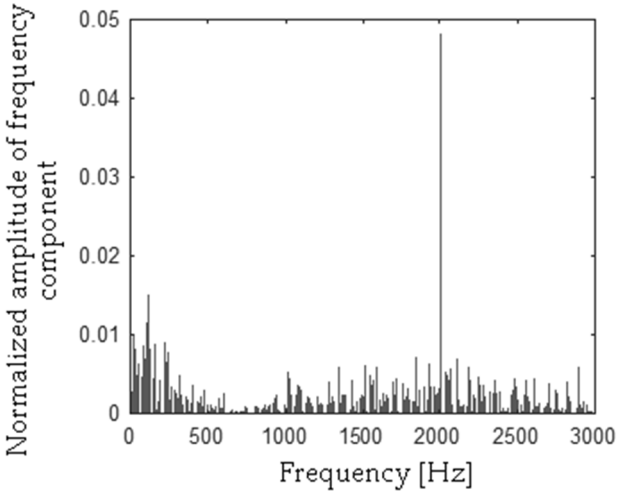

Figure 14. Absolute values of difference of frequency spectra (|**cmbts** − **cmssc**|) using the MSAF-15-MULTIEXPANDED-8-GROUPS.

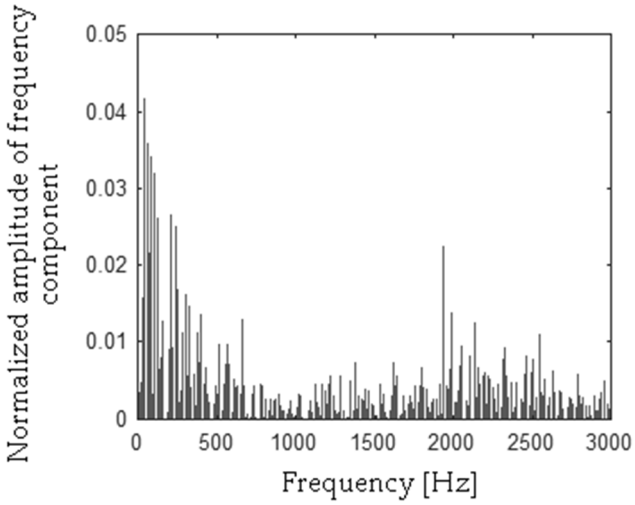

Figure 15. Absolute values of difference of frequency spectra (|**cmdgt** − **hcm**|) using the MSAF-15-MULTIEXPANDED-8-GROUPS.

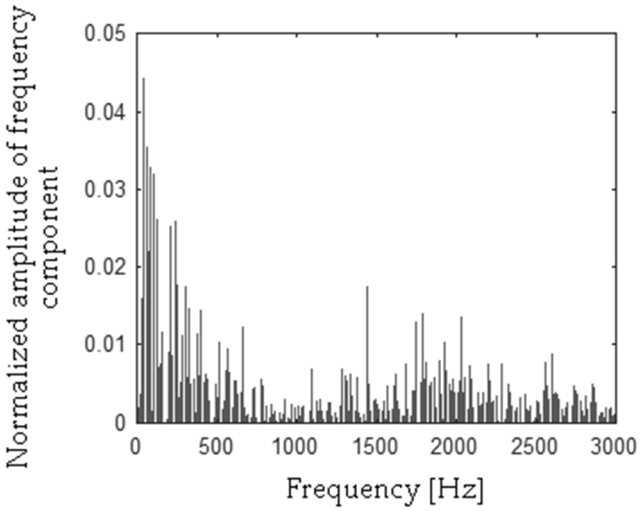

Figure 16. Absolute values of difference of frequency spectra (|**cmdgt** − **cmbrc**|) using the MSAF-15-MULTIEXPANDED-8-GROUPS.

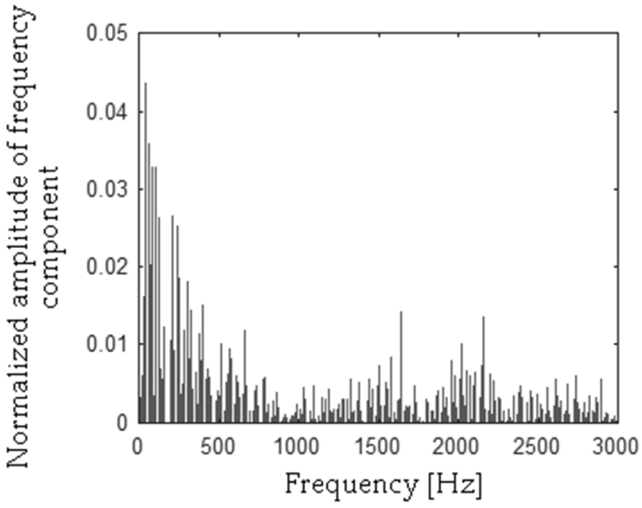

Figure 17. Absolute values of difference of frequency spectra (|**cmdgt** − **cmssc**|) using the MSAF-15-MULTIEXPANDED-8-GROUPS.

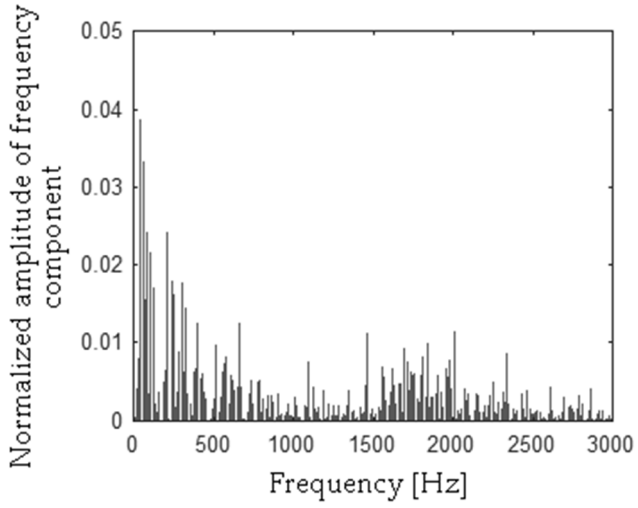

Figure 18. Absolute values of difference of frequency spectra (|**cmdgt** − **cmbts**|) using the MSAF-15-MULTIEXPANDED-8-GROUPS.

Table 1. Computed essential frequency components for vector **hcm** (healthy CM).

Value of Feature			
0.006776	0.011506	0.003938	0.006896
0.003093	0.007896	0.005020	0.006722
0.009599	0.006721	0.034127	0.041374
0.006398	0.001086	0.006096	0.002857
0.004421	0.002796	0.005071	0.005120
0.006776	0.011506	0.003938	0.006896
0.003093	0.007896	0.005020	0.006722

Table 2. Computed essential frequency components for vector **cmbrc** (CM with broken rotor coil).

Value of Feature			
0.005696	0.009528	0.026896	0.004757
0.005556	0.010468	0.026023	0.012042
0.003759	0.009350	0.006706	0.007029
0.005175	0.006020	0.013454	0.003632
0.008541	0.000666	0.005728	0.005724
0.005696	0.009528	0.026896	0.004757
0.005556	0.010468	0.026023	0.012042

Table 3. Computed essential frequency components for vector **cmssc** (CM with shorted stator coils).

Value of Feature			
0.002803	0.002988	0.008468	0.004678
0.004008	0.002770	0.001949	0.006048
0.021171	0.004456	0.005253	0.002312
0.005484	0.005549	0.003781	0.004390
0.005037	0.000740	0.008683	0.004213
0.002803	0.002988	0.008468	0.004678
0.004008	0.002770	0.001949	0.006048

Table 4. Computed essential frequency components for vector **cmbts** (CM with broken tooth on sprocket).

Value of Feature			
0.007080	0.007388	0.006834	0.001410
0.006244	0.007172	0.003946	0.005266
0.002335	0.002029	0.004501	0.007593
0.020768	0.016296	0.016799	0.018125
0.003584	0.011559	0.007451	0.003169
0.007080	0.007388	0.006834	0.001410
0.006244	0.007172	0.003946	0.005266

Table 5. Computed essential frequency components for vector **cmdgt** (CM with damaged gear train).

Value of Feature			
0.002066	0.002245	0.001124	0.000820
0.000845	0.000655	0.002080	0.001540
0.002178	0.001563	0.000810	0.001933
0.002259	0.001234	0.002635	0.003116
0.002729	0.006634	0.000739	0.004000
0.051576	0.012309	0.007059	0.015156
0.019388	0.008816	0.028623	0.016604

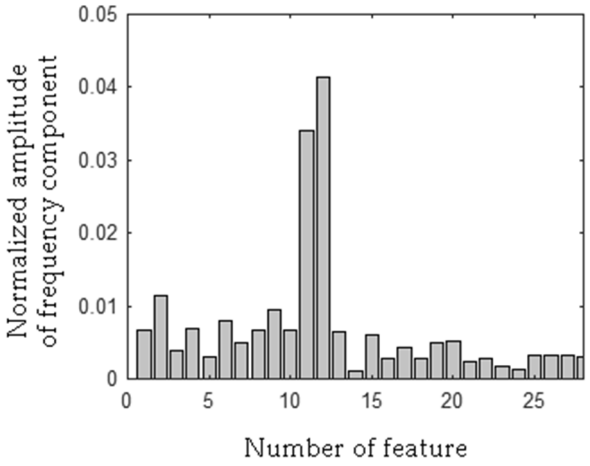

Figure 19. Computed essential frequency components for vector **hcm** (healthy CM).

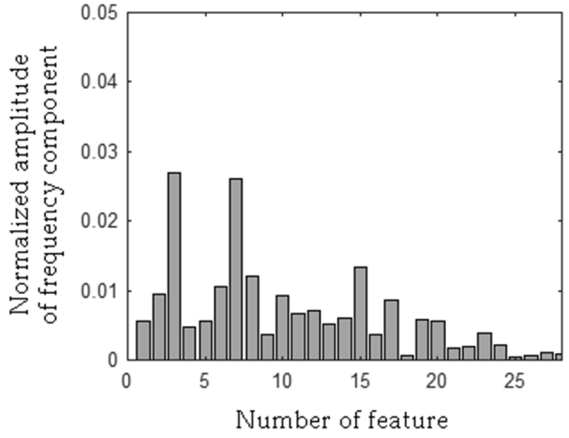

Figure 20. Computed essential frequency components for vector **cmbrc** (CM with broken rotor coil).

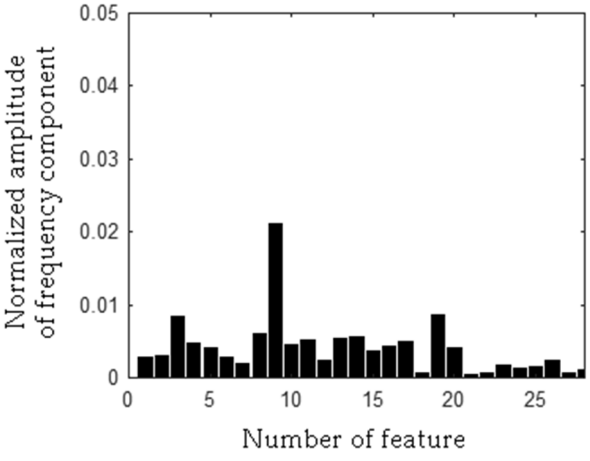

Figure 21. Computed essential frequency components for vector **cmssc** (CM with shorted stator coils).

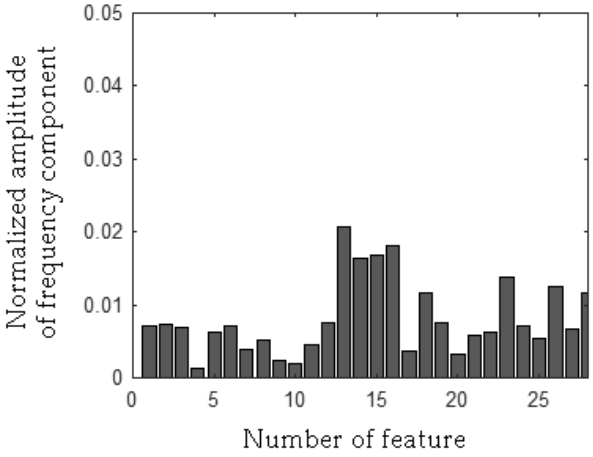

Figure 22. Computed essential frequency components for vector **cmbts** (CM with broken tooth on sprocket).

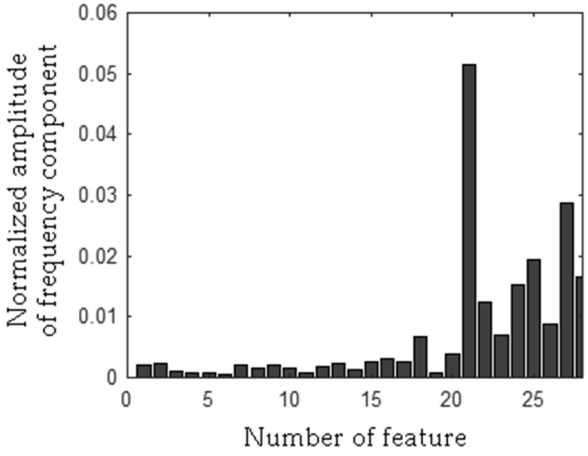

Figure 23. Computed essential frequency components for vector **cmdgt** (CM with damaged gear train).

Found essential frequency components were classified by the NN classifier [35,36], NM classifier, SOM [37], BNN [38–44]. There was possibility to use another classifier such as naive Bayes, support vector machine [45–47], linear discriminant analysis [48], fuzzy classifiers [49,50], and fuzzy c-means clustering [51]. The results of recognition depended on number of found essential frequency components and selected classification method.

2.2. Nearest Neighbour Classifier

A classification step can be achieved by the nearest neighbour (NN) classifier. This method of classification is well-known. It is used in economics, telecommunication, pattern recognition, fault diagnosis, and image recognition. The NN classifier can classify data (linearly separable and non-linearly separable) with high recognition rate. The NN is simple to implement, and it requires a few training feature vectors for proper classification. It uses labels for classification of test feature vectors. The classifier uses metric distance to compare two vectors (training and test feature vectors). There are many distance metrics to compare training and test vector. Distance metrics such as Euclidean, Manhattan, and Minkowski had similar results. In this paper, the classification step was carried out using Manhattan distance (1):

$$d(\mathbf{x}-\mathbf{cmbrc}) = \sum_{i=1}^{1} |(x_i - cmbrc_i)| \quad (1)$$

where d(**x-cmbrc**)—computed distance, unknown test feature vector **x** = [x_{36}, x_{37}, x_{59}, x_{60}, x_{72}, x_{75}, x_{95}, x_{117}, x_{118}, x_{1092}, x_{1094}, x_{1243}, x_{1432}, x_{1433}, x_{1438}, x_{1439}, x_{1442}, x_{1444}, x_{1452}, x_{1455}, x_{1456}, x_{1458}, x_{1471}, x_{1515}, x_{1516}, x_{1518}, x_{1531}, x_{1894}] and training feature vector **cmbrc** = [$cmbrc_{36}$, $cmbrc_{37}$, $cmbrc_{59}$, $cmbrc_{60}$, $cmbrc_{72}$, $cmbrc_{75}$, $cmbrc_{95}$, $cmbrc_{117}$, $cmbrc_{118}$, $cmbrc_{1092}$, $cmbrc_{1094}$, $cmbrc_{1243}$, $cmbrc_{1432}$, $cmbrc_{1433}$, $cmbrc_{1438}$, $cmbrc_{1439}$, $cmbrc_{1442}$, $cmbrc_{1444}$, $cmbrc_{1452}$, $cmbrc_{1455}$, $cmbrc_{1456}$, $cmbrc_{1458}$, $cmbrc_{1471}$, $cmbrc_{1515}$, $cmbrc_{1516}$, $cmbrc_{1518}$, $cmbrc_{1531}$, $cmbrc_{1894}$]. The result of classification was depended on the nearest distance d(). Description of the NN classifier is available in following articles [35,36].

2.3. Nearest Mean Classifier

Similar to the NN classifier, the nearest mean (NM) classifier is also based on computed distance. It uses average feature vector instead of training feature vectors. Average feature vector **afv** is defined as (2)

$$\mathbf{afv} = \frac{1}{p}\sum_{i=1}^{p} y_i \tag{2}$$

where **afv**—average feature vector, p—number of essential frequency components, and y_i—value of essential frequency component with i index.

The nearest distance between test and average feature vector is computed. Next, the label occurring with specific average feature vector is the label for the test feature vector. The NM classifier can classify data with a high recognition rate. For the classification step, the author used Manhattan distance (1).

2.4. Self-Organizing Map

The self-organizing map was used for machine learning. The self-organizing map (SOM) is a clustering method. It does not use labels for classification of test feature vectors. The SOM is an unsupervised neural network. It is used for clustering data, meteorology and oceanography, project prioritization, selection, and failure analysis. For example, the SOM is used for meteorological applications such as climate change analysis, precipitation, snow, wind, air temperature, etc. The SOM analysis has been applied for computed feature vectors of acoustic signals. Similarity between feature vectors depends on the location of features on the two-dimensional map (nodes). The SOM uses training step and testing step. In the training step, weights of nodes are changed (at the beginning, values of weights are random). The author used the following self-organizing map (Figure 24). It was implemented in MATLAB. Description of the SOM is available in the following article [37].

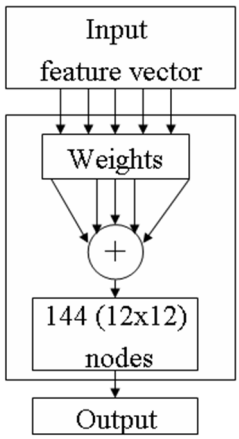

Figure 24. Implemented self-organizing map—144 nodes.

2.5. Backpropagation Neural Network

Backpropagation neural network (BNN) was also used for machine learning. It is a supervised learning method. It is also a well-known method of data classification. It has been used for many applications, such as speaker recognition, image recognition, signal recognition, control, prediction, computer games, robots, etc. The applied backpropagation algorithm has been described in the literature [38–44]. The author implemented a backpropagation neural network (Figure 25).

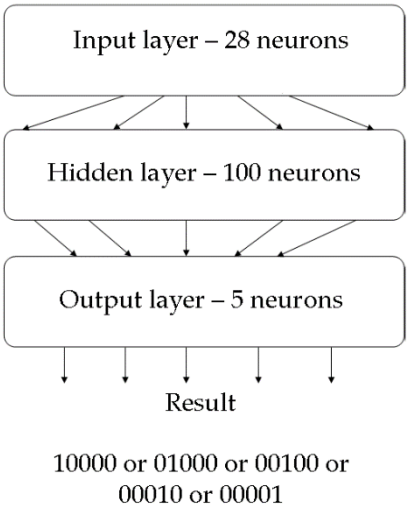

Figure 25. Implemented backpropagation neural network (BNN).

Layers of BNN had following number of neurons: input layer—28, hidden layer—100, output layer—5. The values of output neurons were 10000—healthy CM, 01000—CM with shorted stator coils, 00100—CM with broken rotor coil, 00010—CM with broken tooth on sprocket, and 00001—CM with damaged gear train. More information about BNN can be found in following papers [38–44].

3. Results of Acoustic-Based Fault Diagnosis Technique of the Commutator Motor

Measurements of acoustic signals of commutator motors were conducted in the workshop. The author measured and analysed 5 states of the CM: healthy CM, CM with shorted stator coils (Figure 26a), CM with broken rotor coil (Figure 26b), CM with broken tooth on sprocket (Figure 27), and CM with damaged gear train (Figure 28). Analysed commutator motors had the following parameters: W_{oM} = 1.84 kg, P_{oM} = 500 W, RS_{oM} = 3000 rpm, V_{oM} = 230 V, f_{oM} = 50 Hz, where W_{oM}—weight of the motor, P_{oM}—rated power of the motor, RS_{oM}—rotor speed, V_{oM}—supply voltage of the motor, and f_{oM}—current frequency of the motor.

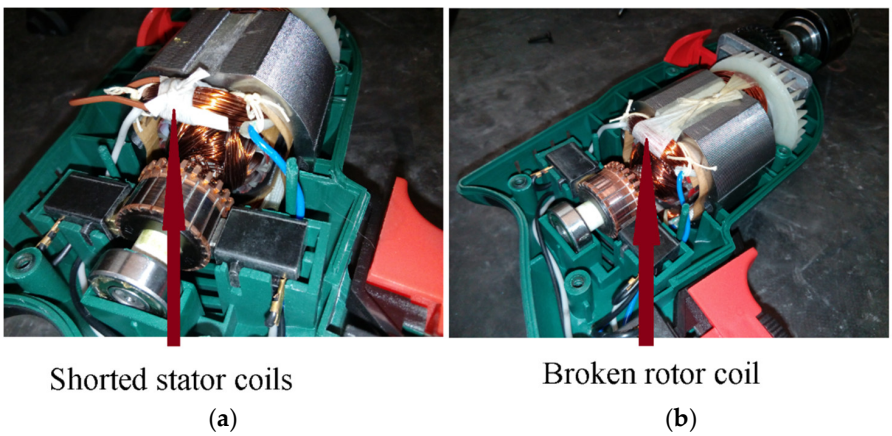

Figure 26. (**a**) CM with shorted stator coils; (**b**) CM with broken rotor coil.

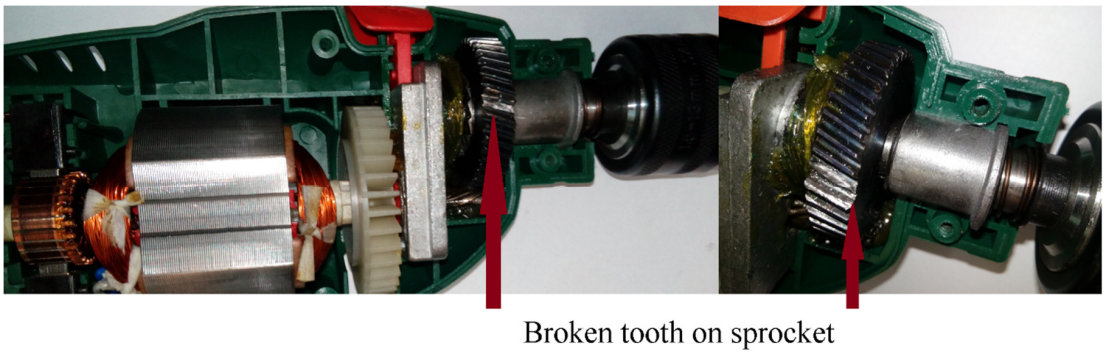

Figure 27. CM with broken tooth on sprocket.

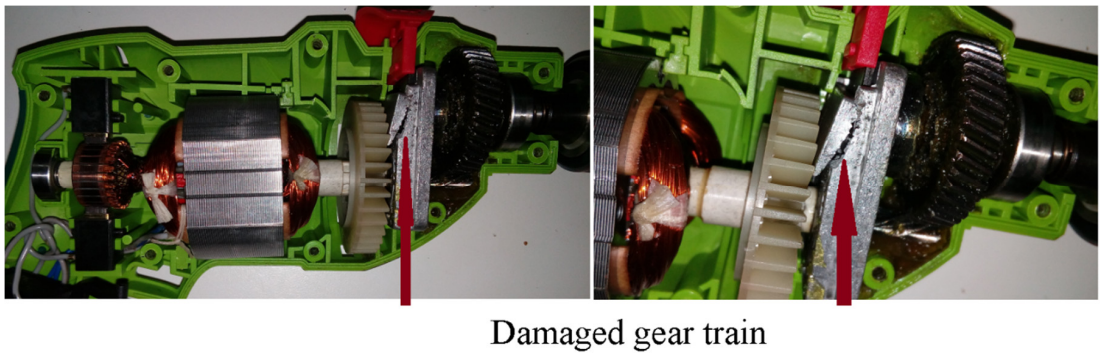

Figure 28. CM with damaged gear train.

The author used 30 one-second training samples for proper pattern creation process. The author used 500 one-second test samples for proper testing process. Training and test samples of the CM were processed and analysed. The author used technique presented in Section 2 for proper fault diagnosis. Acoustic data of the CM were analysed using efficiency of recognition (E_{RCM}). It was defined as (3):

$$E_{RCM} = (N_{TSCMTP})/(N_{ATSCM}) \cdot 100\% \quad (3)$$

where: E_{RCM}—efficiency of recognition of the CM for defined class, N_{TSCMTP}—number of test samples of the CM for defined class tested properly, N_{ATSCM}—number of all test samples of the CM for defined class.

Total efficiency of recognition of the CM (TE_{RCM}) was introduced to evaluate efficiency of recognition of all states of the CM. It was expressed as (4):

$$TE_{RCM} = (E_{RCM1} + E_{RCM2} + E_{RCM3} + E_{RCM4} + E_{RCM5})/5 \quad (4)$$

where TE_{RCM}—total efficiency of recognition of the CM, E_{RCM1}—efficiency of recognition of the healthy CM, E_{RCM2}—efficiency of recognition of the CM with broken rotor coil, E_{RCM3}—efficiency of recognition of the CM with shorted stator coils, E_{RCM4}—efficiency of recognition of the CM with broken tooth on sprocket, and E_{RCM5}—efficiency of recognition of the CM with damaged gear train.

Acoustic signal analysis of the CM is presented in Tables 6–9. The acoustic signal analysis of the CM using the MSAF-15-MULTIEXPANDED-8-GROUPS and the NN are presented in Table 6 (28 analysed frequency components).

Table 6. Acoustic signal analysis of the CM using the MSAF-15-MULTIEXPANDED-8-GROUPS and the NN.

Type of Acoustic Signal	E_{RCM} [%]
Healthy CM	90
CM with broken rotor coil	87
CM with shorted stator coils	94
CM with broken tooth on sprocket	100
CM with damaged gear train	100
	TE_{RCM} [%]
	94.2

Table 7. Acoustic signal analysis of the CM using the MSAF-15-MULTIEXPANDED-8-GROUPS and the NM.

Type of Acoustic Signal	E_{RCM} [%]
Healthy CM	89
CM with broken rotor coil	91
CM with shorted stator coils	93
CM with broken tooth on sprocket	100
CM with damaged gear train	100
	TE_{RCM} [%]
	94.6

Table 8. Acoustic signal analysis of the CM using the MSAF-15-MULTIEXPANDED-8-GROUPS and the SOM.

Type of Acoustic Signal	E_{RCM} [%]
Healthy CM	87
CM with broken rotor coil	86
CM with shorted stator coils	81
CM with broken tooth on sprocket	90
CM with damaged gear train	98
	TE_{RCM} [%]
	88.4

Table 9. Acoustic signal analysis of the CM using the MSAF-15-MULTIEXPANDED-8-GROUPS and the BNN.

Type of Acoustic Signal	E_{RCM} [%]
Healthy CM	85
CM with broken rotor coil	88
CM with shorted stator coils	82
CM with broken tooth on sprocket	91
CM with damaged gear train	99
	TE_{RCM} [%]
	89

The acoustic signal analysis of the CM using the MSAF-15-MULTIEXPANDED-8-GROUPS and the NM are shown in Table 7 (28 analysed frequency components).

The acoustic signal analysis of the CM using the MSAF-15-MULTIEXPANDED-8-GROUPS and the SOM were presented in Table 8 (28 analysed frequency components).

The acoustic signal analysis of the CM using the MSAF-15-MULTIEXPANDED-8-GROUPS and the BNN were presented in Table 9 (28 analysed frequency components).

The method of feature extraction the MSAF-15-MULTIEXPANDED-8-GROUPS and selected classifiers provided high recognition rates (TE_{RCM} in the range of 88.4–94.6%).

The MSAF-15-MULTIEXPANDED-8-GROUPS used 28 frequency components of the CM. The NN classifier and the MSAF-15-MULTIEXPANDED-8-GROUPS provided TE_{RCM} = 94.2%. The NM classifier and the MSAF-15-MULTIEXPANDED-8-GROUPS provided TE_{RCM} = 94.6%. The SOM (self-organizing map) and the MSAF-15-MULTIEXPANDED-8-GROUPS provided TE_{RCM} = 88.4%. The BNN and the MSAF-15-MULTIEXPANDED-8-GROUPS provided TE_{RCM} = 89%.

Self-organizing map and backpropagation neural network are trained. The training is different each time. The NN classifier and the NM classifier had the same results each time. Moreover, feature vectors had small differences between them. The NN classifier and the NM classifier were better for the recognition of close feature vectors.

4. Conclusions

The article presented acoustic-based fault diagnosis technique of the CM. Five states of the CM were considered: healthy CM, CM with broken rotor coil, CM with shorted stator coils, CM with broken tooth on sprocket, and CM with damaged gear train. The method of feature extraction MSAF-15-MULTIEXPANDED-8-GROUPS was described and implemented. Classifiers NN, NM, SOM, and BNN were used for acoustic analysis of the CM.

Analysed values of TE_{RCM} were in the range of 88.4–94.6%. The NM classifier and the MSAF-15-MULTIEXPANDED-8-GROUPS provided TE_{RCM} = 94.6%. The implementation of the proposed fault diagnosis technique had low cost. Laptop and microphones are available for $300. Other types of rotating electric motors (such as DC motors, synchronous motors, induction motors) can also be diagnosed using acoustic analysis.

The proposed acoustic-based fault diagnosis technique has its limitations. If the motor runs too quietly, it is difficult to use the mentioned technique and microphone. However, the presented acoustic-based fault diagnosis technique is appropriate for acoustic signals of rotating motor and other types of acoustic signals (for example acoustic signal of an engine). The proposed acoustic-based fault diagnosis technique can be extended to detect more complicated faults. Future research will focus on the analysis of new feature extraction methods, other types of faults, and other diagnostic signals, such as vibrations.

Funding: This research was funded by AGH University of Science and Technology, grant No. 11.11.120.714.

Acknowledgments: This work has been supported by AGH University of Science and Technology, grant No. 11.11.120.714. The author thanks unknown reviewers for their valuable suggestions.

Conflicts of Interest: The author declares no conflict of interest.

References

1. Li, Z.X.; Jiang, Y.; Hu, C.; Peng, Z. Recent progress on decoupling diagnosis of hybrid failures in gear transmission systems using vibration sensor signal: A review. *Measurement* **2016**, *90*, 4–19. [CrossRef]
2. Kim, K.C. Analysis on Electromagnetic Vibration for Interior Permanent Magnet Synchronous Motor Due to Temperature and Loads. *Adv. Sci. Lett.* **2017**, *23*, 9767–9772. [CrossRef]
3. Zhao, H.M.; Deng, W.; Yang, X.H.; Li, X.M. Research on a vibration signal analysis method for motor bearing. *Optik* **2016**, *127*, 10014–10023. [CrossRef]
4. Moosavian, A.; Najafi, G.; Ghobadian, B.; Mirsalim, M. The effect of piston scratching fault on the vibration behavior of an IC engine. *Appl. Acoust.* **2017**, *126*, 91–100. [CrossRef]
5. Cruz-Vega, I.; Rangel-Magdaleno, J.; Ramirez-Cortes, J.; Peregrina-Barreto, H. Automatic progressive damage detection of rotor bar in induction motor using vibration analysis and multiple classifiers. *J. Mech. Sci. Technol.* **2017**, *31*, 2651–2662. [CrossRef]
6. Armentani, E.; Sepe, R.; Parente, A.; Pirelli, M. Vibro-Acoustic Numerical Analysis for the Chain Cover of a Car Engine. *Appl. Sci.* **2017**, *7*, 610. [CrossRef]
7. Jafarian, K.; Mobin, M.; Jafari-Marandi, R.; Rabiei, E. Misfire and valve clearance faults detection in the combustion engines based on a multi-sensor vibration signal monitoring. *Measurement* **2018**, *128*, 527–536. [CrossRef]

8. Siljak, H.; Subasi, A. Berthil cepstrum: A novel vibration analysis method based on marginal Hilbert spectrum applied to artificial motor aging. *Electr. Eng.* **2018**, *100*, 1039–1046. [CrossRef]
9. Zurita-Millan, D.; Delgado-Prieto, M.; Saucedo-Dorantes, J.J.; Carino-Corrales, J.A.; Osornio-Rios, R.A.; Ortega-Redondo, J.A.; Romero-Troncoso, R.D. Vibration Signal Forecasting on Rotating Machinery by means of Signal Decomposition and Neurofuzzy Modeling. *Shock Vib.* **2016**, *2016*, 1–13. [CrossRef]
10. Martinez, J.; Belahcen, A.; Muetze, A. Analysis of the Vibration Magnitude of an Induction Motor with Different Numbers of Broken Bars. *IEEE Trans. Ind. Appl.* **2017**, *53*, 2711–2720. [CrossRef]
11. Saucedo-Dorantes, J.J.; Delgado-Prieto, M.; Ortega-Redondo, J.A.; Osornio-Rios, R.A.; Romero-Troncoso, R.D. Multiple-Fault Detection Methodology Based on Vibration and Current Analysis Applied to Bearings in Induction Motors and Gearboxes on the Kinematic Chain. *Shock Vib.* **2016**, *2016*, 1–13. [CrossRef]
12. Li, Y.; Chai, F.; Song, Z.X.; Li, Z.Y. Analysis of Vibrations in Interior Permanent Magnet Synchronous Motors Considering Air-Gap Deformation. *Energies* **2017**, *10*, 1259. [CrossRef]
13. Delgado-Arredondo, P.A.; Morinigo-Sotelo, D.; Osornio-Rios, R.A.; Avina-Cervantes, J.G.; Rostro-Gonzalez, H.; Romero-Troncoso, R.D. Methodology for fault detection in induction motors via sound and vibration signals. *Mech. Syst. Signal Process.* **2017**, *83*, 568–589. [CrossRef]
14. Dong, J.N.; Jiang, J.W.; Howey, B.; Li, H.D.; Bilgin, B.; Callegaro, A.D.; Emadi, A. Hybrid Acoustic Noise Analysis Approach of Conventional and Mutually Coupled Switched Reluctance Motors. *IEEE Trans. Energy Convers.* **2017**, *32*, 1042–1051. [CrossRef]
15. Stief, A.; Ottewill, J.R.; Orkisz, M.; Baranowski, J. Two Stage Data Fusion of Acoustic, Electric and Vibration Signals for Diagnosing Faults in Induction Motors. *Elektronika ir Elektrotechnika* **2017**, *23*, 19–24. [CrossRef]
16. Xia, K.; Li, Z.R.; Lu, J.; Dong, B.; Bi, C. Acoustic Noise of Brushless DC Motors Induced by Electromagnetic Torque Ripple. *J. Power Electron.* **2017**, *17*, 963–971. [CrossRef]
17. Sangeetha, P.; Hemamalini, S. Dyadic wavelet transform-based acoustic signal analysis for torque prediction of a three-phase induction motor. *IET Signal Process.* **2017**, *11*, 604–612. [CrossRef]
18. Prainetr, S.; Wangnippanto, S.; Tunyasirut, S. Detection Mechanical Fault of Induction Motor Using Harmonic Current and Sound Acoustic. In Proceedings of the 2017 International Electrical Engineering Congress (iEECON), Pattaya, Thailand, 8–10 March 2017.
19. Uekita, M.; Takaya, Y. Tool condition monitoring for form milling of large parts by combining spindle motor current and acoustic emission signals. *Int. J. Adv. Manuf. Technol.* **2017**, *89*, 65–75. [CrossRef]
20. Baghayipour, M.; Darabi, A.; Dastfan, A. An Experimental Model for Extraction of the Natural Frequencies influencing on the Acoustic Noise of Synchronous Motors. In Proceedings of the 8th Power Electronics, Drive Systems & Technologies Conference (PEDSTC), Mashhad, Iran, 14–16 February 2017; pp. 125–130.
21. Islam, M.R.; Uddin, J.; Kim, J.M. Acoustic Emission Sensor Network Based Fault Diagnosis of Induction Motors Using a Gabor Filter and Multiclass Support Vector Machines. *Ad Hoc Sens. Wirel. Netw.* **2016**, *34*, 273–287.
22. Binojkumar, A.C.; Saritha, B.; Narayanan, G. Experimental Comparison of Conventional and Bus-Clamping PWM Methods Based on Electrical and Acoustic Noise Spectra of Induction Motor Drives. *IEEE Trans. Ind. Appl.* **2016**, *52*, 4061–4073. [CrossRef]
23. Singh, G.; Naikan, V.N.A. Detection of half broken rotor bar fault in VFD driven induction motor drive using motor square current MUSIC analysis. *Mech. Syst. Signal Process.* **2018**, *110*, 333–348. [CrossRef]
24. Aimer, A.F.; Boudinar, A.H.; Benouzza, N.; Bendiabdellah, A. Use of the root-ar method in the diagnosis of induction motor's mechanical faults. *Revue Roumaine des Sciences Techniques, Serie Electrotechnique et Energetique* **2017**, *62*, 134–141.
25. Tian, L.S.; Wu, F.; Shi, Y.; Zhao, J. A Current Dynamic Analysis Based Open-Circuit Fault Diagnosis Method in Voltage-Source Inverter Fed Induction Motors. *J. Power Electron.* **2017**, *17*, 725–732. [CrossRef]
26. Gangsar, P.; Tiwari, R. Analysis of Time, Frequency and Wavelet Based Features of Vibration and Current Signals for Fault Diagnosis of Induction Motors Using SVM. In Proceedings of the ASME Gas Turbine India Conference, Bangalore, India, 7–8 December 2017.
27. Yu, L.; Zhang, Y.T.; Huang, W.Q.; Teffah, K. A Fast-Acting Diagnostic Algorithm of Insulated Gate Bipolar Transistor Open Circuit Faults for Power Inverters in Electric Vehicles. *Energies* **2017**, *10*, 552. [CrossRef]
28. Sun, H.; Yuan, S.Q.; Luo, Y.; Guo, Y.H.; Yin, J.N. Unsteady characteristics analysis of centrifugal pump operation based on motor stator current. *Proc. Inst. Mech. Eng. Part A J. Power Energy* **2017**, *231*, 689–705. [CrossRef]

29. Spanik, P.; Sedo, J.; Drgona, P.; Frivaldsky, M. Real Time Harmonic Analysis of Recuperative Current through Utilization of Digital Measuring Equipment. *Elektronika ir Elektrotechnika* **2013**, *19*, 33–38. [CrossRef]
30. Glowacz, A.; Glowacz, W.; Glowacz, Z. Recognition of armature current of DC generator depending on rotor speed using FFT, MSAF-1 and LDA. *Eksploatacja i Niezawodnosc* **2015**, *17*, 64–69. [CrossRef]
31. Gutten, M.; Korenciak, D.; Kucera, M.; Sebok, M.; Opielak, M.; Zukowski, P.; Koltunowicz, T.N. Maintenance diagnostics of transformers considering the influence of short-circuit currents during operation. *Eksploatacja i Niezawodnosc* **2017**, *19*, 459–466. [CrossRef]
32. Lopez-Perez, D.; Antonino-Daviu, J. Application of Infrared Thermography to Failure Detection in Industrial Induction Motors: Case Stories. *IEEE Trans. Ind. Appl.* **2017**, *53*, 1901–1908. [CrossRef]
33. Resendiz-Ochoa, E.; Osornio-Rios, R.A.; Benitez-Rangel, J.P.; Morales-Hernandez, L.A.; Romero-Troncoso, R.D. Segmentation in Thermography Images for Bearing Defect Analysis in Induction Motors. In Proceedings of the 2017 IEEE 11th International Symposium on Diagnostics for Electrical Machines, Power Electronics and Drives (SDEMPED), Tinos, Greece, 29 August–1 September 2017; pp. 572–577.
34. Munoz-Ornelas, O.; Elvira-Ortiz, D.A.; Osornio-Rios, R.A.; Romero-Troncoso, R.J.; Morales-Hernandez, L.A. Methodology for Thermal Analysis of Induction Motors with Infrared Thermography Considering Camera Location. In Proceedings of the IECON 2016—42nd Annual Conference of the IEEE Industrial Electronics Society, Florence, Italy, 23–26 October 2016; pp. 7113–7118.
35. Dong, S.J.; Luo, T.H.; Zhong, L.; Chen, L.L.; Xu, X.Y. Fault diagnosis of bearing based on the kernel principal component analysis and optimized k-nearest neighbour model. *J. Low Freq. Noise Vib. Act. Control* **2017**, *36*, 354–365. [CrossRef]
36. Godoy, W.F.; da Silva, I.N.; Goedtel, A.; Palacios, R.H.C.; Lopes, T.D. Application of intelligent tools to detect and classify broken rotor bars in three-phase induction motors fed by an inverter. *IET Electr. Power Appl.* **2016**, *10*, 430–439. [CrossRef]
37. Merainani, B.; Rahmoune, C.; Benazzouz, D.; Ould-Bouamama, B. A novel gearbox fault feature extraction and classification using Hilbert empirical wavelet transform, singular value decomposition, and SOM neural network. *J. Vib. Control* **2018**, *24*, 2512–2531. [CrossRef]
38. Lopes, T.D.; Goedtel, A.; Palacios, R.H.C.; Godoy, W.F.; de Souza, R.M. Bearing fault identification of three-phase induction motors bases on two current sensor strategy. *Soft Comput.* **2017**, *21*, 6673–6685. [CrossRef]
39. Negrov, D.; Karandashev, I.; Shakirov, V.; Matveyev, Y.; Dunin-Barkowski, W.; Zenkevich, A. An approximate backpropagation learning rule for memristor based neural networks using synaptic plasticity. *Neurocomputing* **2017**, *237*, 193–199. [CrossRef]
40. Caesarendra, W.; Wijayaa, T.; Tjahjowidodob, T.; Pappachana, B.K.; Weec, A.; Izzat Roslan, M. Adaptive neuro-fuzzy inference system for deburring stage classification and prediction for indirect quality monitoring. *Appl. Soft Comput.* **2018**, *72*, 565–578. [CrossRef]
41. Jia, F.; Lei, Y.G.; Guo, L.; Lin, J.; Xing, S.B. A neural network constructed by deep learning technique and its application to intelligent fault diagnosis of machines. *Neurocomputing* **2018**, *272*, 619–628. [CrossRef]
42. Zhang, W.; Li, C.H.; Peng, G.L.; Chen, Y.H.; Zhang, Z.J. A deep convolutional neural network with new training methods for bearing fault diagnosis under noisy environment and different working load. *Mech. Syst. Signal Process.* **2018**, *100*, 439–453. [CrossRef]
43. Lee, J.H.; Delbruck, T.; Pfeiffer, M. Training Deep Spiking Neural Networks Using Backpropagation. *Front. Neurosci.* **2016**, *10*, 508. [CrossRef] [PubMed]
44. Zajmi, L.; Ahmed, F.Y.H.; Jaharadak, A.A. Concepts, Methods, and Performances of Particle Swarm Optimization, Backpropagation, and Neural Networks. *Appl. Comput. Intell. Soft Comput.* **2018**, *2018*, 1–7. [CrossRef]
45. Johnson, J.M.; Yadav, A. Complete protection scheme for fault detection, classification and location estimation in HVDC transmission lines using support vector machines. *IET Sci. Meas. Technol.* **2017**, *11*, 279–287. [CrossRef]
46. Zhang, C.; Peng, Z.X.; Chen, S.; Li, Z.X.; Wang, J.G. A gearbox fault diagnosis method based on frequency-modulated empirical mode decomposition and support vector machine. *Proc. Inst. Mech. Eng. Part C J. Mech. Eng. Sci.* **2018**, *232*, 369–380. [CrossRef]

47. Widodo, A.; Yang, B.S. Support vector machine in machine condition monitoring and fault diagnosis. *Mech. Syst. Signal Process.* **2007**, *21*, 2560–2574. [CrossRef]
48. Glowacz, A. Diagnostics of Rotor Damages of Three-Phase Induction Motors Using Acoustic Signals and SMOFS-20-EXPANDED. *Arch. Acoust.* **2016**, *41*, 507–515. [CrossRef]
49. Valis, D.; Zak, L. Contribution to prediction of soft and hard failure occurrence in combustion engine using oil tribo data. *Eng. Fail. Anal.* **2017**, *82*, 583–598. [CrossRef]
50. Valis, D.; Zak, L.; Pokora, O.; Lansky, P. Perspective analysis outcomes of selected tribodiagnostic data used as input for condition based maintenance. *Reliab. Eng. Syst. Saf.* **2016**, *145*, 231–242. [CrossRef]
51. Yan, X.P.; Xu, X.J.; Sheng, C.X.; Yuan, C.Q.; Li, Z.X. Intelligent wear mode identification system for marine diesel engines based on multi-level belief rule base methodology. *Meas. Sci. Technol.* **2018**, *29*, 05110. [CrossRef]